Diversity of Nanostructured Self-Assemblies from a pH-Responsive ABC Terpolymer in Aqueous Media

ARTICLE *in* MACROMOLECULES · JANUARY 2008

Impact Factor: 5.8 · DOI: 10.1021/ma070948e

4 AUTHORS, INCLUDING:

Constantinos Tsitsilianis
University of Patras
129 PUBLICATIONS **2,558** CITATIONS

SEE PROFILE

Diversity of Nanostructured Self-Assemblies from a pH-Responsive ABC Terpolymer in Aqueous Media

Constantinos Tsitsilianis,*,† Yuri Roiter,‡ Ilias Katsampas,† and Sergiy Minko*,‡

Department of Chemical Engineering, University of Patras, 26504, Patras, Greece, and Institute of Chemical Engineering and High Temperature Chemical Processes, FORTH/ ICE-HT, and Department of Chemistry and Biomolecular Science, Clarkson University, Potsdam, New York 13699-5810

Received April 24, 2007; Revised Manuscript Received November 26, 2007

ABSTRACT: We report on the diverse self-assembly of the poly(2-vinyl pyridine)-*b*-poly(acrylic acid)-*b*-poly(*n*-butyl methacrylate) (P2VP−PAA−PnBMA) ABC terpolymer in aqueous solutions. This has allowed us to fabricate a range of hierarchically organized nanostructured particles and hydrogels just by tuning both the pH and the concentration of polymer solutions. The multiresponsive molecule demonstrates a unique diversity of structural organizations caused by the combination of the P2VP and PAA building blocks. We found conditions for the formation of thermosensitive centrosymmetric core−shell−corona micelles, compact spheres, polyelectrolyte flowerlike micelles, a charged pH-sensitive 3D network, toroidal nanostructures, and finite size clusters (microgels). The transition between different micelles and the hydrogel was induced via the regulation of electrostatic and hydrophobic interactions in the system.

Introduction

The self-assembly of segmented macromolecules and low-molecular weight amphiphiles (surfactants) is the major physical process of integration of molecules into hierarchical nanostructured materials in natural and synthetic systems. Nature demonstrates how the hierarchical self-organization of molecular building blocks through various intra and/or intermolecular interactions, such as hydrophobic interactions, H-bonding, electrostatic interactions, etc., results in complex supramolecular structures with intelligent functions. In an attempt to mimic nature, macromolecular science has developed bottom-up strategies targeting the fabrication of novel advanced materials for a variety of applications. Central objects in these studies include amphiphilic block copolymers, which combine hydrophilic and hydrophobic segments and self-assemble spontaneously in aqueous solutions. They form nanostructured micelles and/or 3D networks constituting the fundamental categories of synthetic soft materials.

Multiple "crew-cut" micellar morphologies, spheres, rods, lamellae, vesicles, and large compound micelles (LCM) were observed in 1995 by Zhang and Eisenberg for highly hydrophobic polystyrene-poly(acrylic acid) (PS−PAA) block copolymers.[1,2] Such a diversity of micellar structures was achieved simply by varying the relative length of the different blocks, demonstrating that micellar morphologies can be tuned through molecular design. Morphogenic effects in the crew-cut micelles can also be induced by adding ions in the aqueous media[3] and/or by altering the dielectric constant of the medium.[4]

A very rich structural polymorphism was observed in ternary systems consisting of a nonionic amphiphilic PEO−PPO−PEO triblock copolymer.[5] Seven liquid crystalline (birefrigent stiff gels) and two micellar structures resulted from the self-assembly of the polymeric amphiphile in a binary immiscible mixture of water (selective for PEO) and *p*-xylene (selective for PPO).

* Corresponding authors. E-mail: ct@chemeng.upatras.gr (C.T.), sminko@clarkson.edu (S.M.).
† University of Patras and FORTH/ICE-HT.
‡ Clarkson University.

Recently, ABC terpolymers have received much attention due to the anticipation of a higher diversity of self-assembled structures and multifunctionality[6] and therefore new potential applications for them. Indeed, exciting nanostructures were observed in selective solvents, i.e., multicompartment micelles of various morphologies such as centrosymmetric segmental micelles (core−shell−corona),[7,8] noncentrosymmetric segmental micelles (multicore),[9,10] toroids,[11] discs,[12] and bumpy nanospheres.[13] The advantage of the multicompartment micelles is in their potential ability to store, transport, and deliver different drugs in the same capsule to a specific target.[14]

Stimuli-responsive ABC terpolymers which undergo abrupt physical or chemical changes in response to changes of environmental conditions (e.g., temperature, pH, ionic strength) represent a very promising class of synthetic macromolecules.[15,16] These molecules have been attracting increasing interest over the past few years due to their potential applications in gene[17] and drug[18] delivery and as injectable hydroscaffolds for tissue engineering,[19] actuators,[20] etc.

In this article we report on the diverse phase behavior of the poly(2-vinyl pyridine)-*b*-poly(acrylic acid)-*b*-poly(*n*-butyl methacrylate) (P2VP−PAA−PnBMA) ABC terpolymer in aqueous solutions. This multiresponsive molecule demonstrates a unique diversity of structural organizations, caused by the combination of the P2VP and PAA building blocks. We found conditions for the formation of centrosymmetric three-compartment micelles, compact spheres, polyelectrolyte flowerlike micelles with a compartmentalized core, charged 3D networks, toroidal nanostructures, and microgels. The transitions between different micelles and hydrogels were induced by tuning the pH levels in aqueous solutions.

Experimental Part

Polymer Synthesis. The triblock terpolymer was synthesized by "living" anionic polymerization in THF at −78 °C under inert atmosphere. 2-Vinylpyridine, *tert*-butyl acrylate, and *n*-butyl methacrylate were polymerized sequentially by using *sec*-butyl lithium as the initiator in the presence of LiCl. The resulting P2VP-PtBA−PnBMA polymer precursor was subjected to acid hydrolysis with a 5-fold excess of concentrated HCl, at 80 °C by reflux in 1,4

10.1021/ma070948e CCC: $40.75
Published on Web 01/15/2008

dioxane for 12 h. The hydrolysis degree was nearly quantitative as determined by ^{1}H NMR in deuterated MeOH−$CDCl_3$ (3:1) mixture and potentiometric titration using 0.1 N NaOH. The resulting P2VP−PAA−PnBMA was diluted in water and purified by dialysis. Characterization of the terpolymer was performed prior to hydrolysis by GPC, static light scattering, and^1 NMR.

Light Scattering. Static light scattering was carried out using a thermally regulated (±0.1 °C) spectrogoniometer, model SEM RD (Sematech France) equipped with a He−Ne laser (633 nm). The refractive index increments d*n*/d*c* required for the interpretation of the static light scattering measurements were determined using a Chromatic KMX-16 differential refractometer operating at 633 nm. The micelle aggregation number, N_{agg}, was calculated from the apparent molecular weight of the micelles ($N_{agg} = M_{w\ mic}/M_{w\ unim}$).

Dynamic light scattering measurements were performed at 25 °C with a full multiple τ digital correlator (ALV-5000/FAST) with 280 channels. The excitation light source was an argon ion laser (Spectra Physics 2020) operating at 488 nm, with a stabilized power of 30 mW. The correlation functions were analyzed by CONTIN to obtain the distribution of relaxation times and by the method of cumulants to obtain the polydispersity index ($\mu_2/\langle\Gamma\rangle^2$).

Rheology. Rheological measurements were performed at 25 °C on a controlled stress rheometer (Rheometrics SR-200) using a cone/plate geometry (diameter 40 mm). After loading the samples, a rest period of 5 min was applied, in order to erase any shear history effects. The shear stress ramping used to collect the data was 0.3 Pa/s.

Electrophoresis. ζ-Potential measurements were carried out at 25 °C, using a Zetaseizer 5000 (Malvern Instruments Ltd.) equipped with a cell type ZET 5104 (cross beam mode).

Turbidity Measurements. A double beam HITACHI U-2001 UV−vis spectrometer was used for the turbidity measurements. The copolymer solution was placed in a 10 mm path-length quartz cuvette containing a small magnetic bar set in motion with the aid of a miniature magnetic stirrer. The temperature was controlled by a HAAKE K15 water-bath and could be adjusted from 5 to 90 °C with the help of a HAAKE DC1 controller. The optical density was monitored at 490 nm.

Atomic Force Microscopy. AFM images were recorded using a DI MultiMode scanning probe microscope (Veeco Instruments Inc., Woodbury, NY) operating in the tapping mode. Silicon tips Budget Sensors (Innovative Solutions Bulgaria, Sofia, Bulgaria) with a radius of <10 nm, a spring constant of 40 N/m, and a resonance frequency of 250−300 kHz were used. AFM images were recorded in 1 s (1 Hz) at 512 pixel resolution and ~1.7 V amplitude set point. Mica of V-1 grade (Structure Probe, Inc., West Chester, PA) was used as the substrate (discs of 12 mm diameter, freshly cleaved before each spin coating).

Sample Preparation. For the rheology measurements, the solutions were directly prepared to the final desired concentration. A proper amount of polymer (acid form) was weighed in a screw-capped vial. First an equivalent amount of 0.1 N NaOH was added to neutralize the PAA units and then water (Millipore MILLI-Q) to the final volume. The samples were stirred vigorously and heated for 48 h at 100 °C. They were centrifuged several times for short periods during the heating procedure for better solution mixing and removal of bubbles. Subsequently the samples were allowed to cool down to room temperature and were weighed. The concentrations were corrected to take into account possible loss of water (less than 1%) during the heating procedure. Good reproducibility in the rheological properties was found after the above treatment implying that equilibrium conditions were attained.

For the light scattering measurements, an initial solution with a concentration of 0.1 wt % were prepared as follows. A proper amount of polymer (acid form) was weighed in a screw-capped vial and then water (Millipore Milli-Q) was added to the final volume. The solution pH was adjusted by adding HCl or NaOH. The ionic strength of the solutions was adjusted to 0.05 M (NaCl). The samples were stirred and heated for 2 h at 60 °C. This was enough time for full dissolution of the polymer solutions. Several concentrations ranging from 0.1 to 0.001 wt % were prepared by dilution of the initial solution. The samples were left 24 h for equilibration prior the measurements. Finally the solutions were carefully filtered through 0.5 μm Millipore filters.

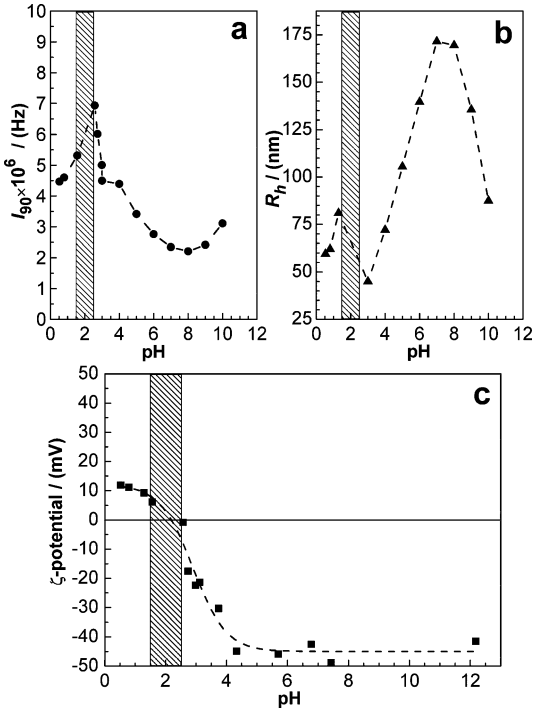

Figure 1. Variation of (a) light scattering intensity (at 90°), (b) apparent hydrodynamic radius, and (c) ζ-potential, as a function of pH for the 0.1 wt % aqueous solution of the $P2VP_{58}-PAA_{924}-P_nBMA_{48}$ triblock terpolymer. The hatched zone is a pH range of the precipitation (two-phase) regime. Lines are provided to guide the reader.

Results and Discussion

The P2VP−PAA−PnBMA triblock terpolymer was synthesized by anionic polymerization followed by acidic selective hydrolysis of the central PtBA block. Proton nuclear magnetic resonance spectroscopy (^{1}H NMR), size-exclusion chromatography (SEC), and static and dynamic light scattering were used to characterize the polymer, designated hereafter as $P2VP_{58}-PAA_{924}-P_nBMA_{48}$ (M_w = 80 000, M_w/M_n = 1.2) , where subscripts denote weight average degree of polymerization of each block.[21] The different nature of the three blocks in aqueous media (P2VP, a weak cationic polyelectrolyte; PAA, a weak anionic polyelectrolyte; PnBMA, hydrophobic polymer) and pH sensitivity of the hydrophilic blocks promised a rich phase behavior in aqueous solutions of this terpolymer.

Static and dynamic light scattering was used to study association phenomena in water. The intensity of the light scattered, I_{90}, and the apparent hydrodynamic radius, R_{happ}, were both obtained at the angle of 90° for the 1 mg/mL polymer solution and are presented in Figure 1 vs pH at 25 °C. I_{90} reflects the aggregation degree of the formed structures. The size of the micelles in this case is affected mainly by the hydrophilic/hydrophobic balance of the terpolymer. Because of the pH-dependent protonation/deprotonation equilibria of the P2VP/PAA blocks, this balance is altered as a function of pH, therefore influencing the association of the macromolecules.

At a very low pH (<2), this association is driven by the intermolecular hydrophobic interactions of the PnBMA blocks. The P2VP block is highly protonated and therefore it is positively charged, while the PAA segments seem to be almost uncharged. As pH increases, a two-phase regime is observed in the vicinity of pH 2 when the polymer precipitates. Inspection

of the ζ-potential of the micelles using electrophoresis (Figure 1c) revealed that in the two phase region, the ζ-potential passes through the zero value, which is consistent with the isoelectric point (IEP) of the $P2VP_{58}-PAA_{924}-P_nBMA_{48}$ ampholitic terpolymer. The IEP of similar copolymer systems depends on the acid to base ratio.[22−24] In the present case, this ratio is very high and results in a shift of IEP to an acidic solution. Therefore, the observed I_{90} maximum at pH 2.5 (upper limit of the precipitation regime) is related to the highest hydrophobicity of the terpolymer.

Above the two phase regime (pH > 2.5), the hydrophilic/hydrophobic balance progressively shifts toward the hydrophilic property as the result of the progressive ionization of the PAA blocks. At pH 8, a minimum in I_{90} was observed, which corresponds to the highest degree of ionization of the PAA segments (maximum hydrophilicity) and, accordingly, to the lowest degree of association. A further pH increase results in partial electrostatic screening of the negative charges along the PAA segments which is due to the ionic strength augmentation. This in turns leads to a slight increase of the association degree.

In Figure 1b, the apparent hydrodynamic radii, R_h, measured for 1 mg/mL $P2VP_{58}-PAA_{924}-PnBMA_{48}$ aqueous solution, appears greater than 45 nm in all cases, suggesting the formation of micellar self-assemblies. The variation of R_h vs pH is more pronounced as compared to the variation of I_{90}, especially above the two-phase regime. This variation is attributed mainly to the short-range repulsive electrostatic interactions which develop along the PAA middle segments and which significantly influence the chain conformation from fully extended at high pH to compact coil at low pH. Indeed, the maximum of R_h is attained near pH 8, where the PAA segments arrive at almost fully extended conformations (the highest degree of ionization). However, it is not only the hydrophobic/hydrophilic balance that governs the association of $P2VP_{58}-PAA_{924}-PnBMA_{48}$ into diverse nanostructured particles; rather, it is also that the specific topology of the different blocks significantly influence the micellar morphology.

Thermosensitive Core−Shell−Corona Micelles. In acidic aqueous media, and especially at pH 1, the three different blocks of the terpolymer exhibit substantially different solubilities: P2VP is highly protonated, behaving as a hydrophilic cationic polyelectrolyte; uncharged PAA is marginally soluble in acidic water (vicinity of Θ point); and the PnBMA segment constitutes the hydrophobic part which drives the polymer to associate.

Static light scattering revealed the formation of micellar self-assemblies as depicted in Figure 2a,b. The angular dependence of the inverse scattering intensity is complex (Figure 2a), at low concentrations is linear whereas at higher concentrations an upward curvature at low angle was observed showing intermicellar interactions. Extrapolation to zero angle (red line in Figure 2b) from the four lower concentrations (exhibiting linear angular dependence) gave an apparent $M_w = 91.1 \times 10^6$ g/mol corresponding to an apparent aggregation number (N_{agg}) of 1138. Such high N_{agg} has been reported recently for micelles formed by PnBA−PAA diblocks at low pH, attributed to low solubility of the uncharged PAA corona chains and likely tendency to clustering.[25]

Dynamic light scattering (DLS) data support the micelle formation observed by the SLS results. In Figure 2c (inset), the relaxation time distributions obtained by the inverse Laplase transformation of the correlation functions from six different polymer concentrations, demonstrate the existence of a single population of micelles of rather broad size polydispersity (i.e., characteristic $\mu_2/\langle\Gamma\rangle^2 = 0.27$) which should be ascribed to the

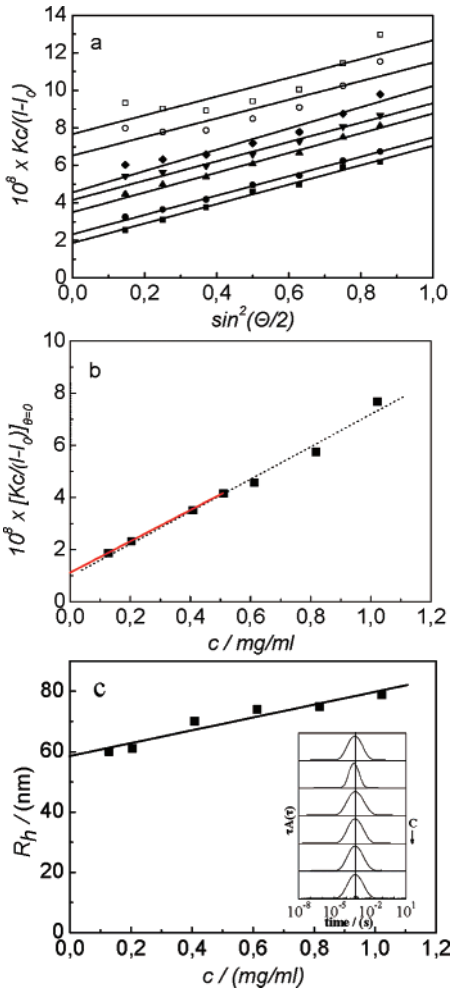

Figure 2. (a) Angular dependence of the inverse scattering intensity for various concentrations in mg/mL: (■) 0.15, (●) 0.2, (▲) 0.4, (▼) 0.5, (♦) 0.6, (○) 0.8, (□) 1.0 (b) concentration dependence of the inverse scattering intensity extrapolated to zero angle and (c) concentration dependence of the apparent hydrodynamic radius (obtained from the relaxation time spectra at different concentrations, inset) for aqueous solutions of the $P2VP_{58}-PAA_{924}-P_nBMA_{48}$ triblock terpolymer at pH 1. Lines represent linear fit.

polymer polydispersity and/or the presence of micellar clusters (see Figure 3). The apparent hydrodynamic radii, R_h, determined through the Stokes−Einstein formula, were plotted versus concentration in Figure 2d. Extrapolation to zero concentration gave $R_h = 58$ nm.

In order to generate deeper insight into the structure of the micelles, atomic force microscopy (AFM) was used. AFM images of micelles spin-coated on the mica substrate from $P2VP_{58}-PAA_{924}-PnBMA_{48}/H_2O$ (pH 1) dilute solutions (0.05 mg/mL) are shown in Figure 3a,b. Spherical micelles and clusters of micelles can be clearly seen in the images. These clusters may be formed through attractive electrostatic interactions of the counterion fluctuations in the periphery of the micelles.[26] Further analysis of the images of isolated micelles (Figure 3c,d) revealed a micellar corona about 15 nm in width which may be attributed to the positively charged P2VP blocks (contour length 14.5 nm). Those end-blocks are located in the periphery of the micelles. Strong attractive interactions among the P2VP positively charged segments and the negatively charged mica also seem to improve the resolution of the outer micellar corona.[27,28] Because of the interaction with the substrate via the P2VP corona, the micellar structure is trapped by the substrate. The sizes of the observed micelles accord well with

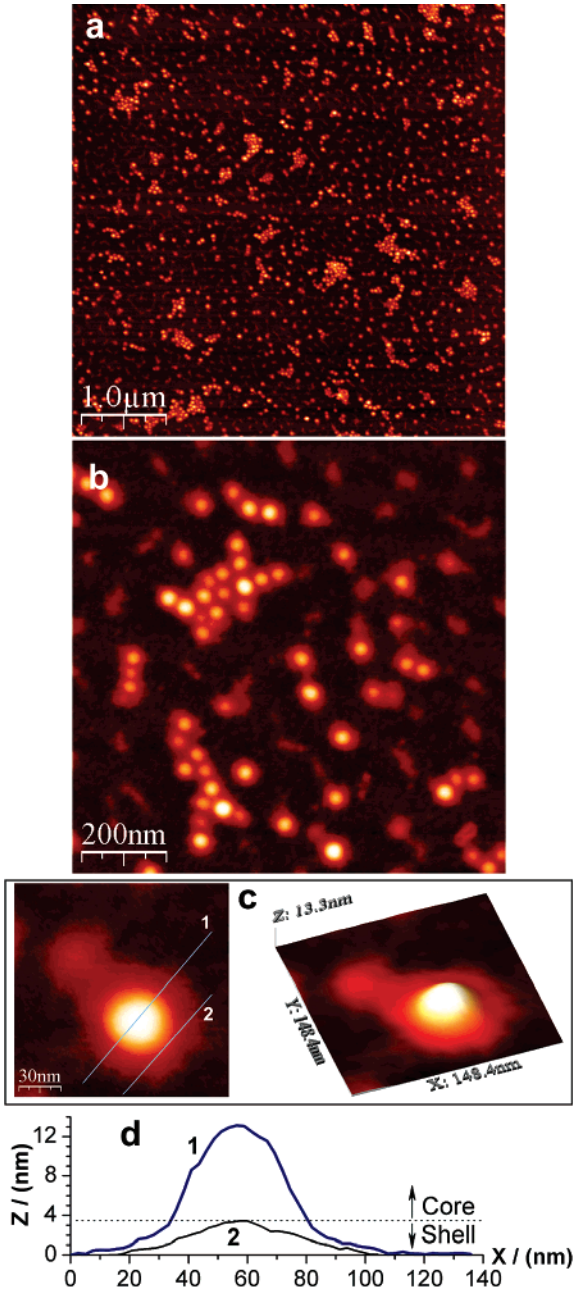

Figure 3. (a−c) AFM imaging from pH 1 (C_p = 0.05 mg/mL); (d) height profile of the micelle along the lines (1,2) in part c.

the micellar diameter obtained through DLS. Although the internal structure of the micelle core cannot be resolved using AFM images, we may speculate that the micelle core consists of segregated hydrophobic PnBMA blocks surrounded by the PAA hydrated inner shell. This centrosymmetric structure is dictated by the topology and the nature of the blocks in the terpolymer. Assuming that the hydrophobic core is a dry compact sphere, the PnBMA core radius can be estimated using simple geometrical considerations by the formula

$$\frac{4\pi}{3}R_c^3 = \frac{N_{agg}N_{PnBMA}M_w}{\rho N_{av}}$$

where N_{PnBMA} is the degree of polymerization of the PnBMA block and ρ (1.05 g/cm^3) is the density of the nBMA repeating unit. R_c was found to be 14.4 nm and the width of the inner PAA shell L_{PAA} = 28.6 nm ($L = R_h - R_c - L_{P2VP}$). Therefore, at pH 1, centrosymmetric three-compartment core−shell−corona

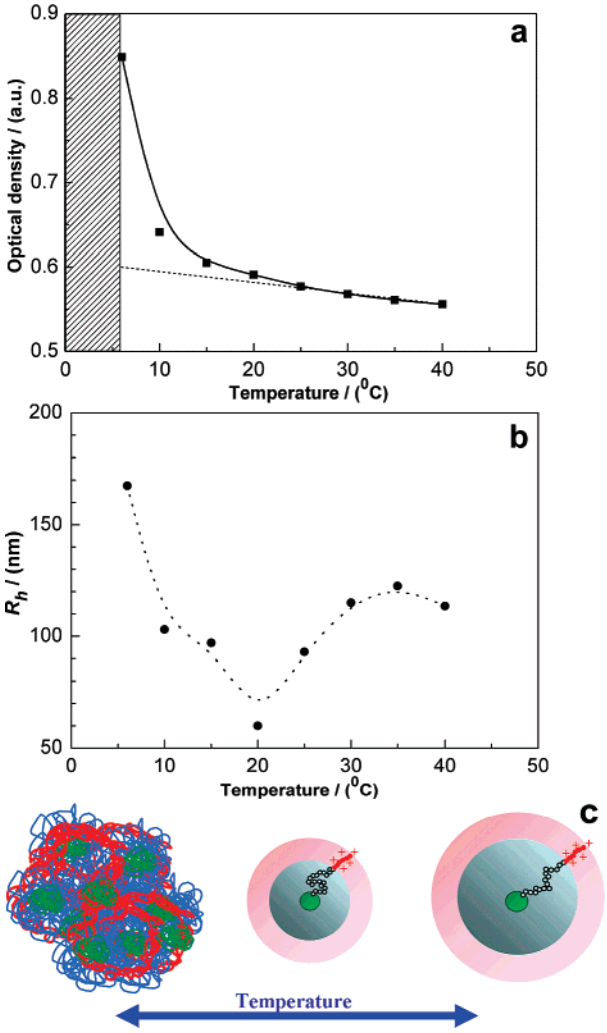

Figure 4. Temperature dependence of (a) optical density and (b) apparent hydrodynamic radius for 0.1 wt % aqueous solution of the $P2VP_{58}-PAA_{924}-P_nBMA_{48}$ triblock terpolymer at pH = 1. The hatched zone denotes the temperature at which the polymer precipitates. Lines are provided to guide the reader. (c) Schematic representation of the micelle thermosensitivity is also presented.

micelles are formed with positively charged corona (as supported by the electrophoresis data: ζ-potential = +10 mV).

Inspection of the possible temperature effects on the core−shell−corona micelles revealed a very interesting and complex behavior. Figure 4 demonstrates the optical density (OD) (Figure 4a) and the apparent R_h of the micelles as a function of temperature. The first observation is an increase of the OD below 20 °C, which leads to polymer precipitation below 6 °C. The remaining relative high turbidity at elevated temperatures is likely due to the presence of some micellar clusters as observed by AFM. This effect could be explained by the thermosensitivity of the PAA blocks of the inner shell of the micelles, which exhibits Θ point (UCST) at 14 °C in 0.2 M HCl aqueous solutions.[29] Provided that the ionic strength is low but not zero, the Θ point could be slightly higher.

A better insight into the temperature response of the micelles can be obtained from the plot of apparent R_h versus T. As seen in Figure 3b, R_h exhibits a minimum at 20 °C, suggesting the existence of two different temperature effects. Below 20 °C, PAA makes the transition to a hydrophobic state, driving the system to phase separation through an intermicellar aggregation. Thus, the increase of R_h with decreasing temperature below 20 °C implies the formation of mesoglobules[30] prior to

precipitation. In this case, the short charged P2VP segments cannot stabilize the micelles effectively.

Above 20 °C, the increase of the micellar size should be attributed to the swelling of the PAA inner shell of the micelles due to the excluded volume effect above the Θ temperature. H-bonding between the acrylic acid moieties that breaks upon heating could also contribute to the observed micelle swelling. Thermosensitivity of a physical gel arisen from the PAA−P2VP−PAA triblock copolymer association in acidic solutions was also attributed to PAA blocks.[31]

Although the observed partial clustering of micelles may introduce some error on the light scattering results (apparent N_{agg}, R_h), direct observations by AFM and the topology of the terpolymer show that centrosymmetric core−shell−corona micelles seem to be formed at pH 1. Such micelles differ from those described in the literature,[32,33] which discusses micelles composed either from two highly incompatible hydrophobic compartments and a nonionic soluble corona[9,34] or those core−shell−corona structures with one hydrophobic core, positively charged shell (or thermo-sensitive shell[35]), and neutral soluble corona.[7] In our case, the micelles are constituted of a hydrophobic core, a pH/thermosensitive hydrophilic inner compartment, and an outer positively charged soluble corona.

Spherical Micellar Nanoparticles. As pH increases, electrostatic interactions between oppositely charged moieties (protonated P2VP and deprotonated PAA) leads to polymer precipitation (1.8 < pH < 2.7). The system again becomes a homogeneous solution above pH 2.7, when the negatively charged repeating units of acrylic acid predominate, as suggested by the negative values of the ζ-potential (Figure 1c).

At pH 3 and 4, the aggregation numbers, determined by SLS (Supporting Information), were 365 and 410, respectively, which are remarkably lower than those observed at pH 1. In addition, the hydrodynamic radii were determined to be 44 and 62 nm, respectively, thereby remaining comparable with those at pH 1. These micellar characteristics should be justified by the higher hydrophilicity of the terpolymer arising from the progressive PAA ionization upon pH enhancement.

In order to come to a deeper understanding of this behavior, we performed reference SLS and DLS experiments with a $P2VP_{58}-PAA_{924}$ diblock copolymer at pH 3. Although this copolymer is comprised of two hydrophilic blocks at this pH, it indeed self-assembles mainly through electrostatic interactions[22,23,31] into compact aggregates with $N_{agg} = 331$ and $R_h = 87$ nm. Therefore, the association of the $P2VP_{58}-PAA_{924}-PnBNA_{48}$ in this pH region proceeds through both electrostatic and hydrophobic interactions. Furthermore, the contribution of the hydrophobic interactions (from the PnBMA segments) results in a more compact structure of the triblock terpolymer than that of the diblock precursor.

AFM images of the structures obtained from pH 4 are shown in Figure 5. Spherical, compact nanoparticles of rather low polydispersity, 50 nm in diameter, were clearly observed on the mica substrate. The positively charged outer corona formed at pH 1 has disappeared at this point and the P2VP segments have entered to the interior of the particles partially interacting with the PAA segments. The ζ-potential was measured to be −40 mV, meaning that the nanoparticles were negatively charged. The particles visualized in a dry state appear compressed, mainly in the *Z*-direction (less in the *X* and *Y* directions) structures. The particles in the dry state have a smaller diameter (50 nm), as compared to those in solution determined by DLS.

Flowerlike Polyelectrolyte Micelles. The size of the micellar nanoparticles at pH 4 is greater than that at pH 3. This size

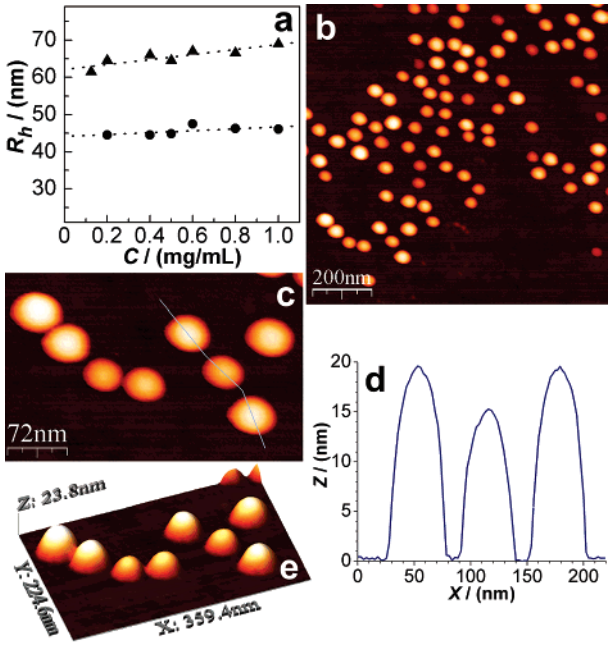

Figure 5. (a) Concentration dependence of the apparent hydrodynamic radius, for the aqueous solution of the $P2VP_{58}-PAA_{924}-P_nBMA_{48}$ triblock terpolymer at pH 3 (●) and 4 (▲). (b,c,e) AFM imaging from (C_p = 0.1 mg/mL) pH 4 and height profile of the micelles along the line in part c.

change should be attributed to the increase of the short-range repulsive electrostatic interactions along the PAA segments (accompanied by a negative ζ-potential enhancement). This effect continues toward complete ionization of the acrylic acid moieties, which occurs close to pH 8 as observed by titration. Simultaneously, the P2VP block is deprotonated, becoming hydrophobic above pH 5. Therefore, upon an increase in pH, the $P2VP_{58}-PAA_{924}-PnBMA_{48}$ terpolymer is transformed from a double-hydrophilic terpolymer into a monohydrophilic terpolymer and more specifically to a hydrophobically end-capped polyelectrolyte, also called a heterotelechelic polyelectrolyte.[36]

The hydrodynamic radius of the associates determined by extrapolation at zero concentration (Figure 6) for the neutralized $P2VP_{58}-PAA_{924}-PnBMA_{48}$ was found to be significantly larger, up to 113 nm, while N_{agg} (Supporting Information) dropped down to 43. This is a direct consequence of the significant shift of the hydrophilic/hydrophobic balance toward hydrophilic behavior and the increased degree of ionization of the PAA blocks, resulting in a stretched conformation of the corona chains.

AFM images of the self-assembled structures obtained at pH 7 and deposited on mica are shown in Figure 6. The copolymer forms spherical micelles with a well resolved extended corona. The configuration of the polyelectrolyte chains in the corona are influenced by two antagonistic factors, (1) the hydrophobic attractive interactions between P2VP and PnBMA end-blocks of the terpolymer that favor chain back folding (formation of loops) and (2) the electrostatic repulsive interactions between the adjacent negative charges along the PAA chains that favor stretching (dangling ends). Although the AFM experiments cannot resolve single loops in the corona, the dangling hydrophobic ends should be visible in the periphery of the corona in the form of spherical small beads, which is not the case as observed by AFM in a recent previous article.[37] Moreover the micelle dimensions obtained from DLS imply that looping predominates. Indeed R_h was found to be half of the contour length of the PAA segments (231 nm) and, more

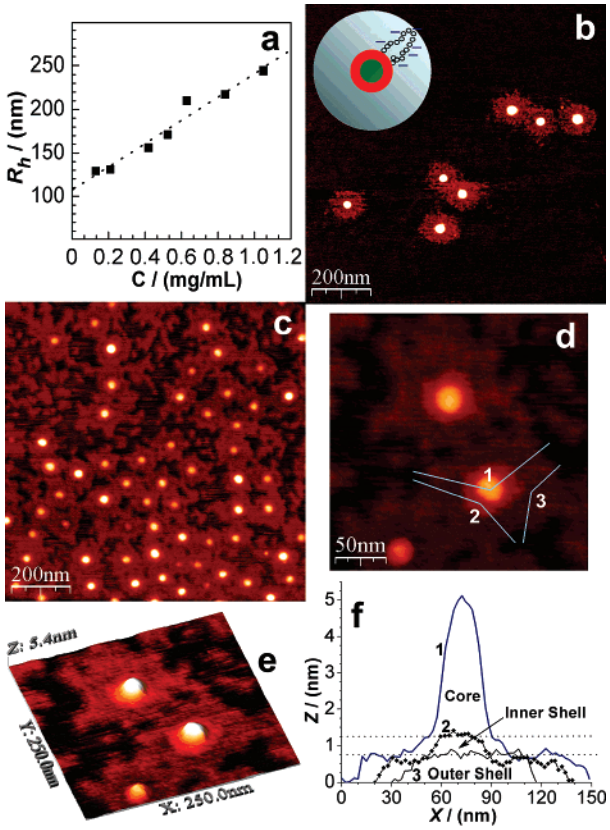

Figure 6. (a) Concentration dependence of the apparent hydrodynamic radius for an aqueous solution of the $P2VP_{58}-PAA_{924}-P_nBMA_{48}$ triblock terpolymer at pH 7. (b−e) AFM images of micelles deposited on mica ($C_p = 0.1$ mg/mL). (f) Height profile of the micelle along the lines 1−3 in part d. Inset of part b, schematic representation of a flowerlike micelle with a compartmentalized core.

importantly, the hydrodynamic radius of the $P2VP_{58}-PAA_{923}$ diblock precursor under the same conditions was estimated to be slightly higher than $2R_h$ of the terpolymer, corroborating the conclusion given above.[36b] Therefore, at pH 6−8, negatively charged polyelectrolyte flowerlike micelles seem to be formed. The micelle core likely has a compartmentalized centrosymmetric structure, consisting of a hydrophobic PnBMA nodule surrounded by a hydrophobic P2VP inner shell (Figure 6b inset).

We address here the important question of whether or not the internal structure of the hydrophobic part, comprising the P2VP and PnBMA segments, exists in an ordered state. Magnification of the AFM images (see Figure 6d,e) and height profile analysis (Figure 6f) revealed the morphology which is consistent with the suggestion of the three compartment core−shell−corona micelle model. The height profiles depicted in Figure 6f were obtained from cross-sections marked in Figure 6d with the solid lines 1−3. The labels of the lines correspond to the labels of the profile plots in Figure 6f. A profile analysis of the dry micelle allowed us to identify three different structural elements of different heights (h): (1) the core $h = 5$ nm, (2) the inner shell $h = 1.2$ nm, and (3) the outer shell $h = 0.8$ nm (the latter two heights are marked with dotted lines in Figure 6f). Although the difference between the height of the inner shell and the height of the outer shell is a small value (0.4 nm), it is well above the accuracy of the AFM instrument in the Z-axis (0.1 nm). This morphology is well reproducible and was found for all the micelles examined. However, AFM cannot provide chemical contrast to aid in identifying the composition of these structural elements. Assuming that the most hydrophobic PnBMA block will be associated first, we could speculate that the PnBMA is in the core and the P2VP hydrophobic segments are located in the inner shell together with some collapsed uncharged AA units placed in the vicinity of the PnBMA segments.[25,38]

The hypothesis concerning the ordered state of the hydrophobic part of the micelles can also be supported by theoretical considerations. The Flory interaction parameter χ_{AC} of the A and C hydrophobic ends of the ABC terpolymer can be calculated using the equation

$$\chi_{AC} = \frac{(\delta_A - \delta_C)^2 V_r}{RT}$$

where δ_A and δ_C are the Hildebrand solubility parameters for the A and C block, respectively, V_r is the reference volume usually taken to be 100 cm^3/mol, and R is the gas constant.[39] The solubility parameter of P2VP and PnBMA, estimated from the Hoy method which uses molar attraction constants and their densities, are 10.0 and 8.7 $(cal/cm^3)^{1/2}$, respectively.[40] Assuming that we have a dry core, the incompatibility factor expressed by the product of $\chi_{AC}N$, where χ_{AC} is the interaction parameter and N is the number of the repeating units ($N_A + N_C$), was calculated to be 30, which favors segregation for a diblock copolymer (AC).[41] Although the two blocks are not covalently bonded (ABC type), this value shows that the system is likely to be in a segregation state, corroborating the AFM observation.

Three-Dimensional Polyelectrolyte Networks. The increase of polymer concentration in the regime of flowerlike polyelectrolyte micelles leads rapidly to a second hierarchical level of association. At pH 6, we observed the formation of micellar strands, as well as irregular clusters as revealed by AFM imaging (Figure 7). The repulsive electrostatic interactions along the PAA blocks can overcome the attractive intramolecular hydrophobic interactions of the chain-ends bridging therefore adjacent flowerlike micelles. The bridges are formed by terpolymer molecules which interconnect the micelles by the two hydrophobic ends of the copolymer. The micelle bridging process continues with concentration into bigger clusters as demonstrated in Figure 7e.

The onset of the network formation was observed through the AFM imaging of structures formed in more concentrated solutions. As shown in Figure 8a, big clusters are interconnected, forming a continuous supramicellar network structure. This is observed to have open unfilled areas which are transformed into a dense gel at the higher polymer concentration (Figure 8b).

The rapid growth of the network was monitored by measuring the zero-shear viscosity as a function of concentration. Steady-shear viscosity experiments were carried out in a stress controlled rheometer as a function of shear stress. Zero-shear viscosity, η_o, was established from the Newtonian plateau at low stress, as seen in Figure 9a. The concentration dependence of η_o is presented in Figure 9b, from which the critical gel concentration was determined to be 0.5 wt % (~5 mg/mL). At 2 wt % concentration, the viscosity has been raised about 8 orders of magnitude with respect to that of the medium. The latter reveals that the studied polymer can act as a very efficient thickener. Oscillatory shear measurements were conducted in the linear viscoelastic regime at low deformation, where the network structure remains intact. These measurements have shown that at 2 wt %, the system behaves as an elastic soft material, since the storage modulus, G', is about 1 order of magnitude greater than the loss modulus, G'', (inset in Figure 9b). Moreover the $G' - G''$ intersection is not visible since it has been shifted to very low frequencies. Therefore the

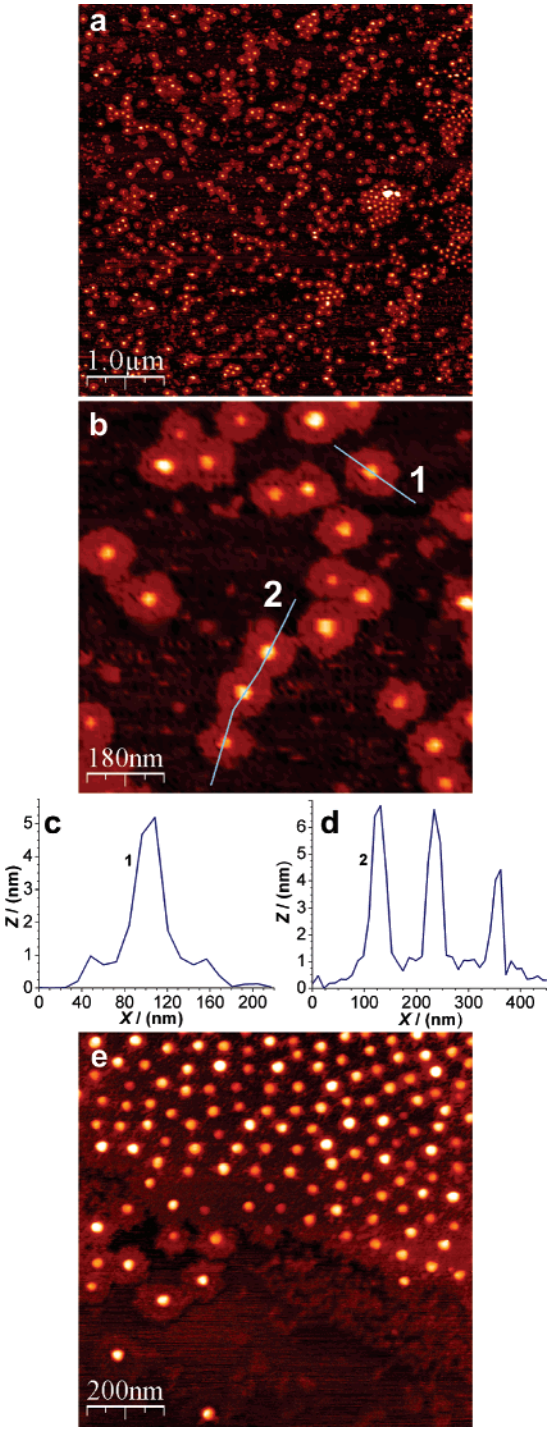

Figure 7. AFM images of structures obtained from $P2VP_{58}-PAA_{924}-P_nBMA_{48}$ aqueous solutions at (a,b) pH 6 (C_p = 0.1 mg/mL), (e) (C_p = 0.5 mg/mL), and (c,d) height profiles along the respective lines in part b.

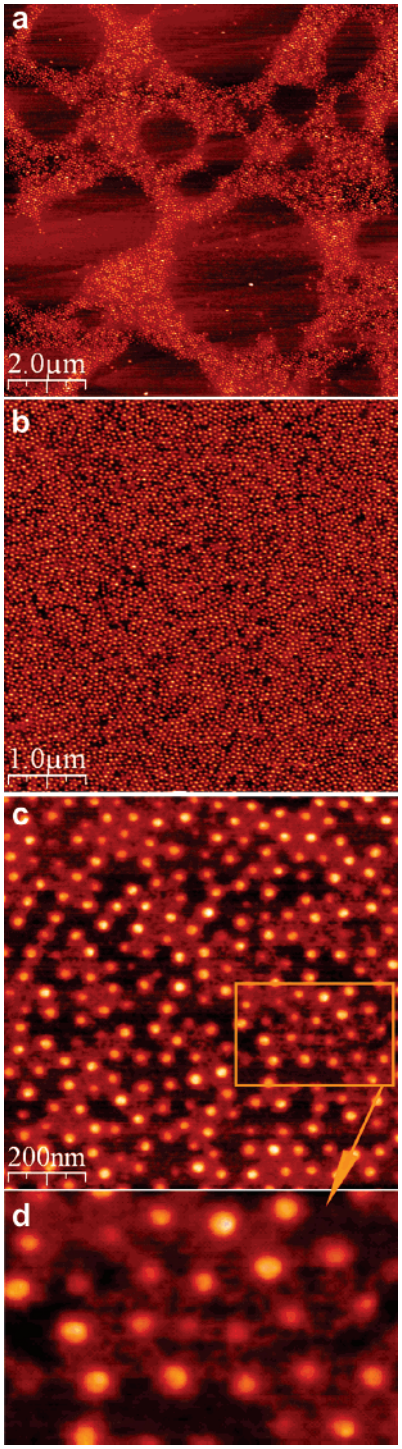

Figure 8. AFM topography of the onset of the micellar network formation of the $P2VP_{58}-PAA_{924}-P_nBMA_{48}$ in an aqueous solution of (a,c,d) C_p= 0.5 mg/mL and (b) C_p = 1.0 mg/mL. Bridging chains are visible in the higher magnification in part d.

characteristic time, t_c, of the fluid is of the order of hundreds of seconds (t_c > 100 s) which is consistent with the features of a strong physical gel.

Another important property of this physically cross-linked soft material is that it exhibits a strong shear thinning effect, as the viscosity drops several orders of magnitude upon shearing (Figure 9b). Provided that the present system works properly at physiological conditions (pH 7.4), it could constitute a good paradigm for an injectable hydrogel in tissue engineering applications.[42]

The above-described physical network consists of hydrophobic cross-links and negatively charged bridging chains. This network is also sensitive to ionic strength. As the pH increases to 10 through the addition of NaOH, the network is disrupted probably by the electrostatic screening of the repulsive interactions along the PAA bridging chains, as observed through AFM microscopy and rheometry. AFM imaging reveals a dramatic change in the network structure (compare parts a and b of Figure 10). The interpretation of these images is complicated by drying the samples, a process which could introduce artifacts. However, the gel is highly viscous, and the deposited film cannot be easily corrupted by capillary forces. We may speculate that the morphology of the deposited film correlates with the 3D

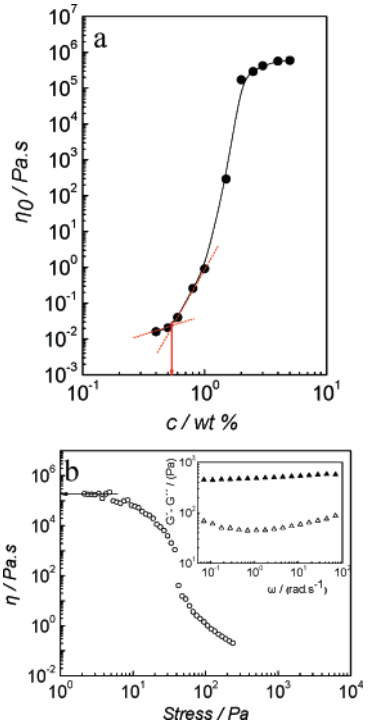

Figure 9. (a) Concentration dependence of zero shear viscosity at pH 7 (red arrow indicates C_{gel}) and (b) steady-state shear viscosity at 2 wt % aqueous polymer solution as a function of applied stress (black arrow shows the zero shear viscosity). The frequency dependence of G' (▲) and G''(△) is shown in the inset of part b.

structure of the gel, and the formation of pores 50−100 nm in diameter in the film is a reflection of the electrostatic screening effect (shrinking PAA chains) in the gel. The resulting lack of network connectivity has dramatic impact on the rheological properties of the system at higher concentrations. As seen in Figure 10c, the Newtonian viscosity decreases by about 4 orders of magnitude as the pH increases from 7.4 to 10.9.

Toroidal Nanostructures. A further addition of NaOH to the diluted micellar solutions in order to increase the pH level induces the structural transformation of flowerlike polyelectrolyte micelles to unexpected toroidal morphologies. As can be observed in Figure 11, the toroids and multimicellar irregular toroidal nanostructures were revealed by AFM experiments after depositing one drop of the 0.1 mg/mL polymer aqueous solution at pH 11. Similar toroidal morphologies have been rarely reported for other synthetic charged block copolymers. For instance, poly(ethylethylene)-*b*-poly(styrene sulfonic acid) (PE−PSS) diblock copolymers form toroidal structures in aqueous solutions of elevated ionic strength.[43] This was attributed to intermicellar electrostatic attractive interactions caused by counterion cloud fluctuations.

Recently, toroidal nanostructures have been observed for poly(acrylic acid)-*b*-poly(methyl acrylate)-*b*-polystyrene (PAA_{99}−PMA_{73}−PS_{66}) triblock terpolymers in a solution of 1:2 by volume THF−water in the presence of divalent 2-2-(ethylenedioxyl)diethylamine (EDDA), (0.5:1 molar ratio of amine to acid).[11] The formation of toroids in this case was attributed exclusively to the specific combination and topology of the three different blocks and the self-attraction of PAA segments by EDDA. In the system presented here, the polymer self-assembles forming toroids without the action of multivalent cations, and therefore the association mechanism should be quite different.

Surprisingly, the toroidal nanostructures illustrated in Figure 11 quite strongly resemble those formed by calf thymus DNA in dilute aqueous solutions after condensation using cobalt−

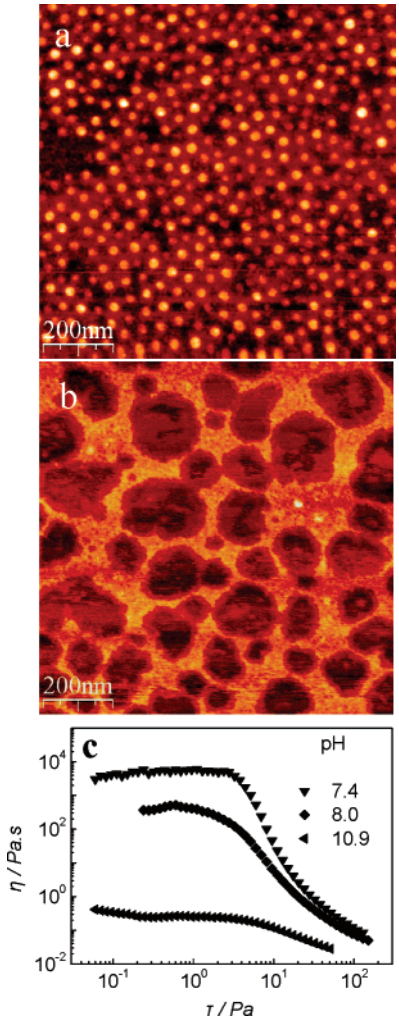

Figure 10. AFM topography of $P2VP_{58}$−PAA_{924}−P_nBMA_{48} polymer aqueous solutions (C_p = 1.5 mg/mL) at (a) pH 7 and (b) pH 10, and (c) the steady-state shear viscosity profile (C_p = 20 mg/mL) at different pH levels.

amine compounds offering trivalent cations.[44] The DNA condensation that results in ordered morphologies of finite size is a well-known phenomenon, occurring through electrostatic intermolecular attractions developed in the presence of multivalent cations. Multivalent cations screen electrostatic repulsions arising from the close packing of a highly charged DNA biopolymer.[45] Nevertheless, mononucleosomal DNA has also been found to aggregate in the presence of NaCl.[46]

As has been predicted theoretically by Manning et al.,[47] an attraction between two parallel polyelectrolyte rods can develop at short distances due to entropy gain by counterions, as they share the volume between the rods. The above considerations seem to fit in our case. The most likely association mechanism is the formation of wormlike cylindrical arrays comprising several PAA chains, with hydrophobic segments at both ends. Hydrophobic segments attract each other, leading to the formation of toroids (unfolding cylinders are clearly visible as a part of multimicellar objects in Figure 11). Intermicellar electrostatic attractions also act in the formation of the multitoroidal nanostructures (Figure 11d−f).

The estimated dimensions of the single toroids (averaged for 50 structures and corrected by size of the AFM tip) are as follows (in a dry state): inner diameter 11 ± 6 nm, outer diameter 32 ± 6 nm, vertical thickness (shrunk upon drying) 1.9 ± 0.3 nm, and volume 1300 ± 300 nm^3; this gives about 25 terpolymer chains per single toroid.

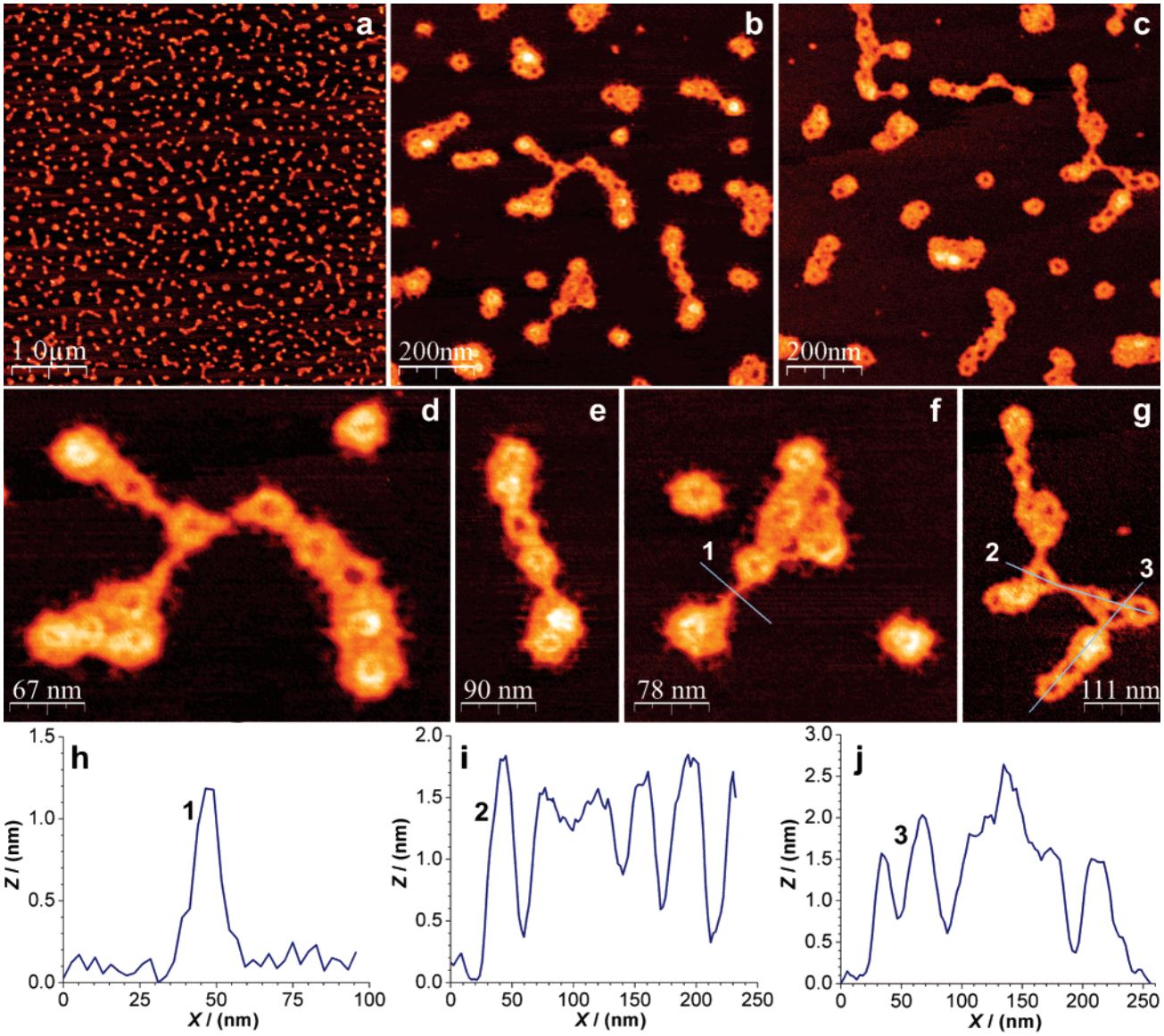

Figure 11. AFM images of toroidal nanostructures obtained from $P2VP_{58}-PAA_{924}-P_nBMA_{48}$ aqueous solutions (C_p = 0.1 mg/mL) at pH 11. (h−j) Height profiles of the toroids along the lines in parts f and g denoted by corresponding numbers.

Finite Size Clusters (Microgels). A further increase in pH to 12 results in one more phase transition in the system, documented by AFM experiments. As seen in Figure 12, spherical objects with a high polydispersity by diameter, which reached up to 2 μm, were deposited on the mica substrate from a dilute aqueous solution. Similar morphologies, called large compound micelles (LCM), were reported by Eizenberg et al. in 1995. In that case, the LCM was prepared with highly hydrophobic $PS_{200}-PAA_4$ diblock copolymers (1.5 wt % PAA) in DMF−water mixtures and isolated through dialysis against deionized water. Transmission electron microscopy, which was used for the elucidation of the LCM internal structure, showed that they were composed of inverted micelles (PAA core, PS shell), with hydrophilic neutralized short PAA chains at the surface stabilizing the micelles. Even though the aggregates observed in Figure 12 resemble the LCM of PS−PAA, they should exhibit completely different internal structures since they are composed of highly hydrophilic (PAA 90 wt %) $P2VP_{58}-PAA_{924}-PnBMA_{48}$ triblock terpolymers. We may speculate that these structures represent the so-called "finite size clusters" predicted theoretically for polyelectrolytes with sticky (hydrophobic) ends in water.[48] According to the theory, the finite-sized clusters of a telechelic polyelectrolyte are composed of

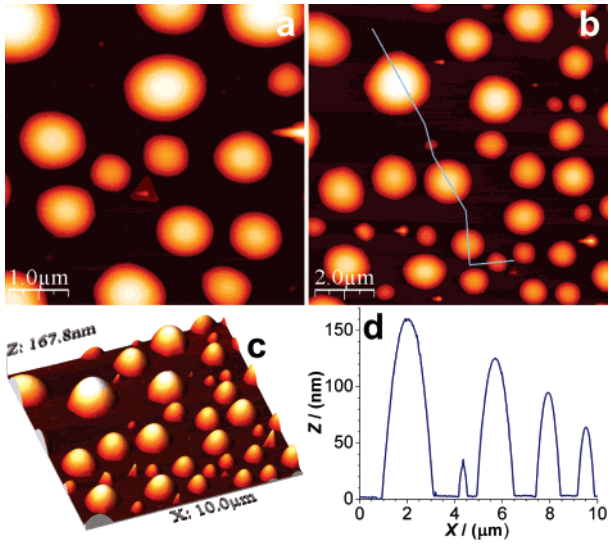

Figure 12. AFM topography of microgel (a−c) obtained from $P2VP_{58}-PAA_{924}-P_nBMA_{48}$ aqueous solutions (C_p = 0.1 mg/mL) at pH 12. (d) Height profile of the microgels along the lines in part b.

elastically active chains which are cross-linked at their hydrophobic ends. These clusters are thermodynamically stable, due to the interplay between the energy of attraction of stickers and the Coulomb interaction, combined with the contribution from the translational entropy of counterions.

More precisely, clusters (microgels) of large size and high polydispersity were predicted to exist at a low degree of chain ionization. In this case, both the Coulomb energy of charges and the entropy of counterions are decreased and the attractions between the stickers induce the size increase of the clusters.[48] Indeed, at pH 12, the short-range electrostatic repulsive interactions along the corona PAA chains decrease due to the electrostatic screening by the excess of ions (elevated ionic strength). This fact favors the appearance of the clusters observed in Figure 12, which is in good agreement with the theoretical predictions.[48]

Conclusions

A $P2VP_{58}-PAA_{924}-PnBMA_{48}$ ABC terpolymer was explored in aqueous dilute solutions at different environmental conditions by light scattering and AFM. Because of the specific architecture (topology, relative block lengths) and the nature of the blocks (positively charged/hydrophobic, negatively charged, hydrophobic) of the macromolecule, an unprecedented structural diversity and multifunctionality was observed by varying only the pH level.

Polymeric micelles of various morphologies have been also observed in aqueous medium for analogues, however much more hydrophobic (more than 50 wt % in hydrophobic content) synthetic copolymers.[1−4,11,12,49] To the best of our knowledge, the present system constitutes the first paradigm in which a highly hydrophilic terpolymer exhibits a very rich diversity in its self-assembly.

Because of a variety of interactions (either intra- or intermolecular), such as hydrophobic and electrostatic (either attractive or repulsive), among the three polymeric segments, a large variety of self-assemblies were formed by pH switching.

At pH 1, positively charged centrosymmetric core−shell−corona micelles, which were sensitive to temperature as well, were observed. Temperature changes induce a dual effect. Below 20 °C, a micelle to mesoglobule transition occurs prior to precipitation, while above 20 °C, swelling of the marginally solubilized inner shell leads to a significant size augmentation. This kind of micelle could be an important aid for the design of multiloaded carriers for drug delivery. As pH increases to pH 8, compact spheres and finally polyelectrolyte flowerlike micelles with a compartmentalized hydrophobic core were observed. Loop to bridge transitions lead rapidly to the formation of a negatively charged 3D network. This supramolecular structure offers another functionality (e.g., injectable reversible hydrogels). At pH 11, toroidal nanostructures were formed. Finally, at pH 12 finite size clusters in the form of microgels were observed.

Acknowledgment. I.K would like to thank FORTH/ICE-HT for financial support. S.M and Y.R acknowledge financial support from the NSF Award CTS 0456548.

Supporting Information Available: Refractive index increments data and angular dependence of the inverse scattering intensity for various concentrations of the $P2VP_{58}-PAA_{924}-P_n$-BMA_{48} triblock terpolymer. This material is available free of charge via the Internet at http://pubs.acs.org.

References and Notes

(1) Zhang, L.; Eisenberg, A. *Science* **1995**, *268*, 1728.
(2) Zhang, L.; Eisenberg, A. *J. Am. Chem. Soc.* **1996**, *118*, 3168.
(3) Zhang, L.; Yu, K.; Eisenberg, A. *Science* **1996**, *272*, 1777.
(4) Choucair, A.; Eisenberg, A. *Eur. Phys. J. E.* **2003**, *10*, 37.
(5) Alexandridis, P.; Olsson, U.; Lindman, B. *Langmuir* **1998**, *14*, 2627.
(6) Bates, F. S.; Fredrickson, G. H. *Phys. Today* **1999**, 32.
(7) (a) Gohy, J.-F.; Willet, N.; Varshney, S.; Zheng, J.-Y.; Jerome, R. *Angew. Chem., Int. Ed.* **2001**, *40*, 9214. (b) Stepanek, M.; Matejicek, P.; Humpolickova, I.; Prochazka, K. *Langmuir* **2005**, *21*, 10783.
(8) Zhou, Z.; Li, Z.; Zen, Y.; Hillmyer, M. A.; Lodge, T. P. *J. Am. Chem. Soc.* **2003**, *125*, 10182.
(9) Li, Z.; Kesselman, E.; Talmon, Y.; Hillmyer, M. A.; Lodge, T. P. *Science* **2004**, *306*, 98.
(10) Kubowicz, S.; Banssard, J.-F.; Lutz, J. F.; Thunemann, A. F.; Berlepsch, H.; Laschewsky, A. *Angew. Chem., Int. Ed.* **2005**, *44*, 5262.
(11) Pochan, D. J.; Chen, Z.; Cui, H.; Hales, K.; Qi, K.; Wooley, K. L. *Science* **2004**, *306*, 94.
(12) Li, Z.; Chen, Z.; Hales, K.; Qi, K.; Wooley, K. L.; Pochan, D. J. *Langmuir* **2005**, *21*, 7533.
(13) Zheng, R.; Liu, G.; Yan, Y. *J. Am. Chem. Soc.* **2005**, *127*, 15358.
(14) Lodge, T. P.; Rasdal, A.; Li, Z.; Hillmyer, M. A. *J. Am. Chem. Soc.* **2005**, *127*, 17608.
(15) Gil, E.S.; Hudson, S. M. *Prog. Polym. Sci.* **2004**, *29*, 1173.
(16) Rodriguez-Hernandez, J.; Checot, F.; Gnanou, Y.; Lecommandoux, S. *Prog. Polym. Sci.* **2005**, *30*, 691.
(17) Benns, J. M.; Choi, J.; Mahato, R. I.; Park, J.; Kim, S. W. *Bioconjugate Chem.* **2000**, *11*, 637.
(18) Shin, H.; Ruhé, P. Q.; Miko, A. G.; Jansen, J. A. *Biomaterials* **2003**, *24*, 3201.
(19) Burdick, J. A.; Anseth, K. S. *Biomaterials* **2002**, *23*, 4315.
(20) Beebe, D. J.; Moore, J. S.; Bauer, J. M.; Yu, Q.; Liu, R. H.; Devadoss, C.; Jo, B.-H. *Nature* **2000**, *404*, 588.
(21) Katsampas, I.; Roiter, Y.; Minko, S.; Tsitsilianis, C. *Macromol. Rapid Commun.* **2005**, *26*, 1371.
(22) Sfika, V.; Tsitsilianis, C. *Macromolecules* **2003**, *36*, 4983.
(23) Sfika, V.; Tsitsilianis, C.; Kiriy, A.; Gorodyska, G.; Stamm, M. *Macromolecules* **2004**, *37*, 9551.
(24) Luo, L.; Eisenberg, A. *Angew. Chem., Int. Ed.* **2002**, *41*, 1001.
(25) Colombani, O.; Ruppel, M.; Burkhardt, M.; Drechsler, M.; Schumacher, M.; Gradzielski, M.; Schweins, R.; Müller, A. H. E. *Macromolecules* **2007**, *40*, 4351.
(26) Grohn, F.; Antonietti, M. *Macromolecules* **2000**, *33*, 5938.
(27) Gorodyska, G.; Kiriy, A.; Minko, S.; Tsitsilianis, C.; Stamm, M. *Nano Lett.* **2003**, *3*, 365.
(28) Kiriy, A.; Gorodyska, G.; Minko, S.; Tsitsilianis, C.; Jaeger, W.; Stamm, M. *J. Am. Chem. Soc.* **2003**, *125*, 11202.
(29) Silberberg, A.; Eliassaf, J.; Katchalsky, A. *J. Polym. Sci.* **1957**, *23*, 259.
(30) Kujawa, P.; Tanaka, F.; Winnik, F. M. *Macromolecules* **2006**, *39*, 3048.
(31) Bossard, F.; Tsitsilianis, C.; Yannopoulos, S.; Petekidis, G.; Sfika, V. *Macromolecules* **2005**, *38*, 2883.
(32) Riess, G. *Prog. Polym. Sci.* **2003**, *28*, 1107.
(33) Gohy, J.-F. *Adv. Polym. Sci.* **2005**, *190*, 65.
(34) Kriz, J.; Masar, B.; Plestil, J.; Tuzar, Z.; Pospisil, H.; Doskocilova, D. *Macromolecules* **1998**, *31*, 41.
(35) Patrickios, C. S.; Forder, C.; Armes, S. P.; Billingham, N. C. *J. Polym. Sci., Part A: Polym. Chem.* **1997**, *35*, 1181.
(36) (a) Tsitsilianis, C.; Katsambas, I.; Sfika, V. *Macromolecules* **2000**, *33*, 9054. (b) Katsambas, I.; Tsitsilianis, C. *Macromolecules* **2005**, *38*, 1307.
(37) Gotzamanis, G. T.; Tsitsilianis, C.; Hadjiyannakou, S. C.; Patrickios, G. S.; Lupitskyy, R.; Minko, S. *Macromolecules* **2006**, *39*, 678.
(38) Stepanek, M.; Prochazka, K.; Brown, W. *Langmuir* **2000**, *16*, 2502.
(39) Hildebrand, J. H.; Scott, R. L. *The Solubility of Non-Electrolytes*, 3rd ed.; Reinhold: New York, 1959.
(40) Brandrup, J., Immergut, E. H., Grulke, E. A., Eds. *Polymer Handbook*; Wiley-Interscience Publications: New York, 1999.
(41) Leibler, L. *Macromolecules* **1980**, *13*, 1602.
(42) Bronich, T. K.; Bontha, S.; Shlyakhtenko, L. S.; Bromberg, L.; Hatton, A.; Kabanov, A. V. *J. Drug Targeting* **2006**, *14*, 357.
(43) Förster, N.; Hermsdorf, W.; Leubem, H.; Schnablegger, M.; Regenbrecht, S.; Akari, S. *J. Phys. Chem. B* **1999**, *103*, 6657.
(44) Deng, H.; Bloomfield, V. A. *Biophys. J.* **1999**, *77*, 1556.
(45) Bloomfield, V. A. *Curr. Opin. Struct. Biol.* **1996**, *6*, 334.
(46) Wissenburg, P.; Odijk, T.; Cirkel, P.; Mandel, M. *Macromolecules* **1994**, *28*, 3215.
(47) Ray, J.; Manning, G. S. *Langmuir* **1994**, *10*, 2450.
(48) Potemkin, J. I.; Vasilevskaya, V. V.; Khokhlov, A. B. *J. Chem. Phys.* **1999**, *111*, 2809.
(49) Liu, F.; Eisenberg, A. *J. Am. Chem. Soc.* **2003**, *125*, 15059.

MA070948E